ELSEVIER

Materials Science and Engineering A328 (2002) 14–25

MATERIALS SCIENCE & ENGINEERING A

www.elsevier.com/locate/msea

A mathematical model for the dissolution of stoichiometric particles in multi-component alloys

F.J. Vermolen [a,*], C. Vuik [a], S. van der Zwaag [b,c]

[a] *Department of Applied Mathematical Analysis, Delft University of Technology, Mekelweg 4, 2628 CD Delft, The Netherlands*
[b] *Laboratory of Materials Science, Delft University of Technology, Rotterdamse weg 137, 2628 AL Delft, The Netherlands*
[c] *Netherlands Institute for Metals Research (N.I.M.R.), Rotterdamse weg 137, 2628 AL Delft, The Netherlands*

Received 18 December 2000; received in revised form 18 May 2001

Abstract

A general model for the dissolution of stoichiometric particles in multi-component alloys is proposed and analysed. We introduce the concept of mass-conserving solutions and give a self-similar solution for the resulting Stefan-problem. Furthermore, we show that particle dissolution in multi-component alloys can under certain circumstances be approximated by a model for particle dissolution in binary alloys. Subsequently, we propose a numerical method to solve the coupled dissolution problem. We end with some examples of hypothetical applications from metallurgy.

Keywords: Multi-component alloy; Particle dissolution; Diffusion; Vector-valued Stefan problem; Self-similar solution

1. Introduction

In the thermal processing of both ferrous and non-ferrous alloys, homogenisation of the existing microstructure by annealing at such a high temperature that unwanted precipitates are fully dissolved, is required to obtain a microstructure suited to undergo heavy plastic deformation as an optimal starting condition for a subsequent precipitation hardening treatment. Such a homogenisation treatment, to name just a few examples, is applied in hot-rolling of Al killed construction steels, HSLA steels, all engineering steels, as well as aluminium extrusion alloys. Although precipitate dissolution is not the only metallurgical process taking place, it is often the most critical of the occurring processes. The minimum temperature at which the annealing should take place can be determined from thermodynamic analysis of the phases present. The minimum annealing time at this temperature, however, is not a constant but depends on particle size, particle geometry, particle concentration, overall composition etc.

Due to the scientific and industrial relevance of being able to predict the kinetics of particle dissolution, many models of various complexity [1–17] have been presented and experimentally validated. In recent years, the simpler models covering binary and ternary alloys have been extended to cover multi-component particles [18–20]. These advanced models cover a range of physical assumptions concerning the dissolution conditions and the initial microstructure. Furthermore, mathematical implications (such as a possible bifurcation of the solution, monotonicity of the solution and well-posedness) are addressed and mathematically sound extensions to the case of n compound particles, with proven theorems concerning existence of mass-concerning solutions and solution bounds, have been derived.

The current paper does not aim at being mathematically rigorous but merely aims at being descriptive about the implications of the developed mathematics of these more complex models. First we formulate the model for particle dissolution in multi-component alloys. Subsequently, we give asymptotic solutions for both the planar and spherical particle. This asymptotic solution is used to verify numerical computations. Furthermore, we show that the multi-component problem (a 'vector-valued' Stefan problem) can be approximated

* Corresponding author. Tel.: +31-15-278-7298; fax: +31-15-278-7209.
E-mail address: f.j.vermolen@its.tudelft.nl (F.J. Vermolen).

0921-5093/02/$ - see front matter
PII: S0921-5093(01)01652-5

by a binary problem ('scalar' Stefan problem) under certain circumstances. Next, we give a numerical scheme to solve the mathematical problem for more general cases. Subsequently, some test-cases are shown using some hypothetical experimental data. We end up with a discussion and some conclusions.

2. Basic assumptions in the model

We consider a particle of a multi-component β-phase surrounded by a 'matrix' of phase α, of uniform or non-uniform composition. The boundary between the β-particle and α-matrix is referred to as the interface. The metal is divided into cells in which a particle of phase β dissolves in a α-matrix. Particle dissolution is assumed to proceed by subsequent steps [9,11], decomposition of the particle, crossing of the interface by atoms from the particle and long-distance diffusion in the α-phase. We assume in this work that the first two mechanisms proceed sufficiently fast with respect to long-distance diffusion. Hence, the interfacial concentrations are those predicted by thermodynamics (local equilibrium). In [20], we considered the dissolution of a stoichiometric particle in a ternary alloy. The hyperbolic relationship between the interfacial concentrations for ternary alloys is derived using a three-dimensional Gibbs space. For the case that the particle consists of n chemical elements apart from the atoms that form the bulk of the β-phase, a generalisation to a n-dimensional Gibbs hyperspace has to be made. The Gibbs surfaces become hypersurfaces. We expect that similar consequences follow and that hence the hyperbolic relation between the interfacial concentrations remains valid for the general stoichiometric particle in a multi-component alloy. We denote the chemical species by Sp_i, $i\in\{1,\ \ldots,\ n+1\}$. We denote the stoichiometry of the particle by $(Sp_1)_{m_1}\ (Sp_2)_{m_2}\ (Sp_3)_{m_3}\ (\ldots)\ (Sp_n)_{m_n}$. The numbers m_1, m_2, …, are stoichiometric constants. We denote the interfacial concentration of species i by c_i^{sol} and we use the following hyperbolic relationship for the interfacial concentrations.

$$(c_1^{\mathrm{sol}})^{m_1}(c_2^{\mathrm{sol}})^{m_2}(\ldots)(c_n^{\mathrm{sol}})^{m_n}=K=K(T). \tag{1}$$

The factor K is referred to as the solubility product. It depends on temperature T according to an Arrhenius relationship.

We denote the position of the moving interface between the β-particle and α-phase by $S(t)$. Consider a one-dimensional domain, i.e. there is one spatial variable, which extends from 0 up to M. Since particles dissolve simultaneously in the metal, the concentration profiles between consecutive particles may interact and hence soft-impingement occurs. This motivates the introduction of cells of finite size over whose boundary there is no flux. Hence, the cell size M is finite. For cases of low overall concentrations in the alloy, the cell size M may be large and the solution resembles the case where M is infinite. The latter case can be treated easily with (semi) explicit expressions. The spatial co-ordinate is denoted by r, $0\le S(t)\le r\le M$. This domain is referred to as $\Omega(t):=\{r\in\mathbb{R}:0\le S(t)\le r\le M\}$. The α-matrix where diffusion takes place is given by $\Omega(t)$ and the β-particle is represented by the domain $0\le r<S(t)$. Hence for each alloying element, we have for $r\in\Omega(t)$ and $t>0$ (where t denotes time)

$$\frac{\partial c_i}{\partial t}=\frac{D_i}{r^a}\frac{\partial}{\partial r}\left\{r^a\frac{\partial c_i}{\partial r}\right\},\quad \text{for } i\in\{1,\ \ldots,\ n\}. \tag{2}$$

Here D_i and c_i, respectively, denote the diffusion coefficient and the concentration of the species i in the α-rich phase. We assume that diffusion of each alloying element is independent of the presence of the other alloying elements. Hence, we set all cross-diffusion coefficients equal to zero. We expect this to be a good approximation for most (dilute) commercial alloys. Furthermore, experiments with differential scanning calorimetry by Chen et al. [15] support this assumption. Hence, Eq. (2) is a simplification of the more general multi-component diffusion equation as stated by Kirkaldy and Young [21]. The geometry is planar, cylindrical and spherical for $a=0$, 1 and 2, respectively. Let c_i^0 denote the initial concentration of each element in the α-phase, i.e. we take as initial conditions (IC) for $r\in\Omega(0)$

$$(\mathrm{IC})\begin{cases}c_i(r,0)=c_i^0(r) & \text{for}\quad i\in\{1,\ \ldots,\ n\}\\ S(0)=S_0\end{cases}$$

We omit the more general case in [18] where we consider the possibility of two simultaneously dissolving/growing particles. At a boundary not being an interface, i.e. at M or when $S(t)=0$, we assume no flux through it, i.e.

$$\frac{\partial c_i}{\partial r}=0,\quad \text{for}\quad i\in\{1,\ \ldots,\ n\}. \tag{3}$$

Furthermore, at the moving interface $S(t)$ we have the 'Dirichlet boundary condition' c_i^{sol} for each alloying element. The concentration of element i in the particle is denoted by c_i^{part}, this concentration is fixed at all stages. This assumption follows from the constraint that the stoichiometry of the particle is maintained during dissolution in line with Reiso et al. [16]. The dissolution rate (interfacial velocity) is obtained from a mass-balance. Summarised, we obtain at the interface for $t>0$ and $i,\ j\in\{1,\ \ldots,\ n\}$.

$$\left.\begin{aligned} & c_i(S(t),t) = c_i^{\mathrm{sol}} \\ & \frac{\mathrm{d}S}{\mathrm{d}t} = \frac{D_i}{c_i^{\mathrm{part}} - c_i^{\mathrm{sol}}} \frac{\partial c_i}{\partial r}(S(t),t) \end{aligned}\right\} \Rightarrow \frac{D_i}{c_i^{\mathrm{part}} - c_i^{\mathrm{sol}}} \frac{\partial c_i}{\partial r}(S(t),t) = \frac{D_j}{c_j^{\mathrm{part}} - c_j^{\mathrm{sol}}} \frac{\partial c_j}{\partial r}(S(t),t). \tag{4}$$

The right part of above equations follows from local mass-conservation of the components. Above formulated problem falls within the class of Stefan-problems, i.e. diffusion with a moving boundary. Since we consider simultaneous diffusion of several chemical elements, it is referred to as a 'vector-valued Stefan problem'. The unknowns in above Eqs. (3) and (4) are the concentrations c_i, interfacial concentrations c_i^{sol} and the interfacial position $S(t)$. All concentrations are non-negative. For a mathematical overview of Stefan problems we refer to the textbooks of Crank [22], Chadam and Rasmussen [23] and Visintin [24].

3. Analysis of the model

In this section, we consider some general mathematical properties of the dissolution model. For the diffusion equation with appropriate boundary conditions there exists exactly one solution c_i that is continuous at least up to the first and second derivative with respect to, respectively, time t and position r. Protter and Weinberger [25] prove that these smooth solutions satisfy a maximum principle, i.e. the global extremes of c_i occur either at the boundaries ($r = S(t)$, $r = M$) or at $t = 0$. For the vector-valued Stefan problem the interfacial concentrations are coupled via the right part of Eq. (4).

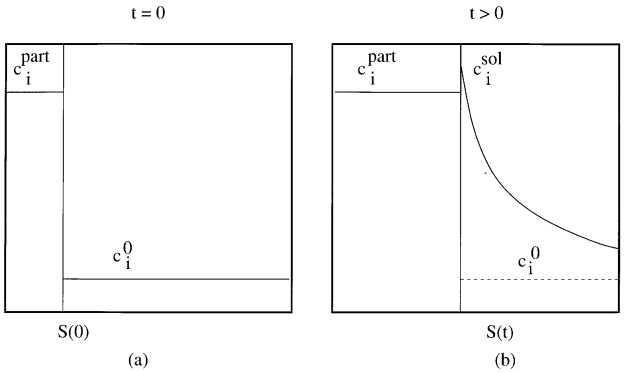

Fig. 1. The hypothetical case $c_i^0 < c_i^{\mathrm{part}} < c_i^{\mathrm{sol}}$ which gives growth of the α-phase and violation of the mass-balance, (a) shows the initial situation and (b) shows a situation at some time $t > 0$.

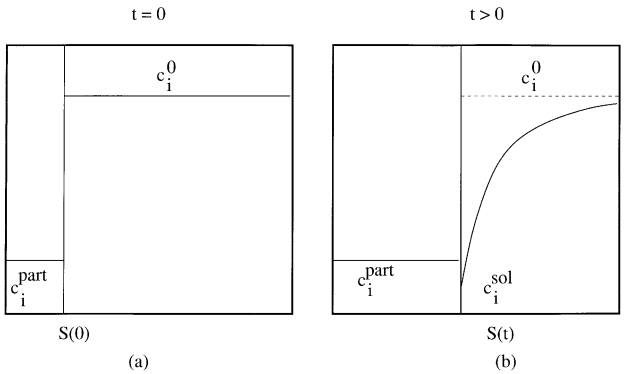

Fig. 2. The hypothetical case $c_i^{\mathrm{sol}} < c_i^{\mathrm{part}} < c_i^0$ which gives growth of the α-phase and violation of the mass-balance, (a) shows the initial situation and (b) shows a situation at some time $t > 0$.

3.1. Mass conserving solutions

We require that the total mass of all chemical elements is constant in the whole dissolution cell, i.e. over $0 \le r \le M$. Further, let c_i^0 be constant over $\Omega(0)$, then

$$\int_0^M c_i(r,t) r^a \,\mathrm{d}r = c_i^{\mathrm{part}} \frac{S_0^{a+1}}{a+1} + c_i^0 \frac{M^{a+1} - S_0^{a+1}}{a+1}.$$

Subtraction of

$$\int_0^M c_i^0 r^a \,\mathrm{d}r = c_i^0 (M^{a+1}/a+1)$$

from both sides of above equation gives

$$\int_0^M (c_i(r,t) - c_i^0) r^a \,\mathrm{d}r = (c_i^{\mathrm{part}} - c_i^0) \frac{S_0^{a+1}}{a+1}. \tag{5}$$

All solutions of the Stefan-problem have to satisfy this condition. We use an intuitive argument to show that some Stefan-problems do not have solutions that satisfy mass-conservation and hence are *ill-posed*. A mathematical theorem is rigorously proven in [18].

Suppose that $c_i^0 < c_i^{\mathrm{part}} < c_i^{\mathrm{sol}}$, i.e. the interfacial concentration exceeds the initial concentration (see Fig. 1). From $t = 0$ the interfacial concentration can increase (build up) only due to transport of atoms from the particle to the interface and matrix (since concentration gradients and reactions are absent initially). This implies that the total number of atoms of the alloying elements in the particle must decrease.

On the other hand from the maximum principle of the diffusion equation follows that $\frac{\partial c_i}{\partial r}(S(t),t) < 0$. Hence, the total number of atoms of the alloying element in the matrix increases. Furthermore, we have $c_i^{\mathrm{part}} - c_i^{\mathrm{sol}} < 0$, which implies $\frac{\mathrm{d}S}{\mathrm{d}t} > 0$, hence the total number of atoms of the alloying elements in the particle increases. This gives a contradiction.

Both the interfacial movement due to growth and the increase of the total number of atoms of the alloying element are sketched in Fig. 1. Mass can not be conserved for this case.

Similar arguments can be used to show that the other case $c_i^{\mathrm{sol}} < c_i^{\mathrm{part}} < c_i^0$ also violates mass-conservation (see Fig. 2). This statement can be generalised in the following result.

Claim. *Let all concentrations be non-negative, then the following combinations give non-conserving solutions in the sense of* Eq. (5),

- $c_i^{sol} < c_i^{part} < c_i^0$,
- $c_i^0 < c_i^{part} < c_i^{sol}$ (*see* Figs. 1 and 2 *for both cases*).

This result is used to reject possible (numerical) unphysical solutions that result from the vector-valued Stefan-problem. Furthermore, negative concentrations are unphysical and hence rejected.

3.2. An asymptotic solution for the planar case

Here we consider the case of a α-particle dissolving in an unbounded domain, i.e. $M = \infty$ and $\Omega(t)$ is unbounded at the right side. Furthermore, the domain is planar, i.e. $a = 0$ in Eq. (2). The interfacial concentrations c_i^{sol} satisfy Eq. (1). For completeness we start with the derivation of the self-similar solution for the one-component problem. As far as we know, Weber was the first to derive such solution for the freezing problem [26].

3.2.1. The one-component problem

Suppose that the interface concentration of a certain component is known, say $c(S(t),\ t) = c^{\mathrm{sol}}$ for a same component. Then, we have to solve the following problem (we refer to this problem as (P1)).

$$(\mathrm{P1})\begin{cases} \dfrac{\partial c}{\partial t} = D\dfrac{\partial^2 c}{\partial r^2} \\ \dfrac{\mathrm{d}S}{\mathrm{d}t} = \dfrac{D}{c^{\mathrm{part}} - c^{\mathrm{sol}}}\dfrac{\partial c}{\partial r}(S(t),\ t) \\ c(S(t),t) = c^{\mathrm{sol}} \\ c(r,\ 0) = c^0 = c(\infty,\ t), \qquad S(0) = (S_0) \end{cases}.$$

Here, we omit the subscript i. As in [18] we search a self-similar solution for the function $c = c(r,\ t)$ and for $S = S(t)$ we state a square-root behaviour as a function of time. Trial of $c = c(\frac{r - S_0}{2\sqrt{Dt}})$ shows that these expressions satisfy the differential equations in (P1). Setting $\eta = \frac{r - S_0}{2\sqrt{Dt}}$ gives the following differential equation for $c = c(\eta)$ with general solution

$$-\eta c' = c'' \Rightarrow c = c(\eta) = A\ \mathrm{erfc}(\eta) + B.$$

The complementary error function is defined as

$$\mathrm{erfc}(x) := 1 - \mathrm{erf}(x) = (2/\pi)\int_x^{\infty} \mathrm{e}^{-y^2}\,\mathrm{d}y.$$

Trial of $S = S_0 + k\sqrt{t}$, substitution of $c(S(t),\ t) = c^{\mathrm{sol}}$ into above solution and use of the initial condition gives

$$A\ \mathrm{erfc}\left(\frac{k}{2\sqrt{D}}\right) + B = c^{\mathrm{sol}}$$
$$\lim_{x\to\infty}\mathrm{erfc}(x) = 0 \Rightarrow B = c^0$$

Solving for A and B gives the *Neumann*-solution as derived in [27]

$$c(r,\ t) = \frac{c^0 - c^{\mathrm{sol}}}{\mathrm{erf}\ c(\frac{k}{2\sqrt{t}})}\,\mathrm{erfc}\left(\frac{r - S_0}{2\sqrt{Dt}}\right) + c^0$$

Above solution and $S = S_0 + k\sqrt{t}$ are substituted into Eq. (4) to give the following expression for the constant k.

$$\frac{c^0 - c^{\mathrm{sol}}}{c^{\mathrm{part}} - c^{\mathrm{sol}}}\sqrt{\frac{D}{\pi}}\frac{\mathrm{e}^{-k^2/4D}}{\mathrm{erfc}(\frac{k}{2\sqrt{D}})} = \frac{k}{2} \tag{6}$$

above equation is solved for k using a standard zero-point iteration method. The physical model in which the solubilities are coupled hyperbolically, see Eq. (1), is valid only for the dilute regime [21]. Therefore, in most cases we have $c_i \ll c_i^{\mathrm{part}}$. Hence, in general we have $\left|\frac{c^{\mathrm{sol}} - c^0}{c^{\mathrm{part}} - c^{\mathrm{sol}}}\right| \ll 1$. From above equation it can be shown that k is then approximated by (we refer to [27] for more detail)

$$k = -2\frac{c^{\mathrm{sol}} - c^0}{c^{\mathrm{part}} - c^{\mathrm{sol}}}\sqrt{\frac{D}{\pi}}. \tag{7}$$

This gives the classical formula for the interfacial velocity that has been obtained by Aaron and Kotler [10] using Laplace transforms

$$\frac{\mathrm{d}S}{\mathrm{d}t} = -\frac{c^{\mathrm{sol}} - c^0}{c^{\mathrm{part}} - c^{\mathrm{sol}}}\sqrt{\frac{D}{\pi t}}. \tag{8}$$

We remark that the derivation of above equation using the Laplace transform contains the assumption that the interface moves very slowly compared with the rate of diffusion, i.e. it is a so-called 'frozen profile' approach. For most cases of particle dissolution in solid metals and alloys, the frozen profile approach is a reasonable approximation. Therefore, above approximation is used in the present paper for the extension to the multi-component problem.

3.2.2. The multi-component problem

As a trial solution for the planar case in a semi-unbounded region, we take the interfacial concentrations to be constant (these concentrations are not constant in time for other cases). Eq. (4) has to be fulfilled, hence combined with Eq. (6) one obtains the following system of non-linear Equations to be solved for k and c_i^{sol} for $i \in \{1,\ \ldots,\ n\}$.

$$\begin{cases} \dfrac{c_i^{\mathrm{sol}} - c_i^0}{c_i^{\mathrm{part}} - c_i^{\mathrm{sol}}}\sqrt{\dfrac{D_i}{\pi}}\dfrac{\mathrm{e}^{-k^2/(4D_i)}}{\mathrm{erf}\ c(k/2\sqrt{D_i})} = \dfrac{k}{2} \quad \text{for} \\ i \in \{1,\ \ldots,\ n\}, (c_1^{\mathrm{sol}})^{m_1}(c_2^{\mathrm{sol}})^{m_2}(c_3^{\mathrm{sol}})^{m_3}(\ldots) = K. \end{cases} \tag{9}$$

The first set of Eq. (9) represents the coupling between the interfacial concentrations of the alloying elements. Due to the non-linear nature of above equations, the solution is in general not unique. Above set of equations provides an exact solution for the 'vector valued' Stefan-problem in the parameters k and c_1^{sol}, c_2^{sol}, …, c_n^{sol}. Due to its complexity, we rely on numerical solution techniques to obtain its solution. This solution is referred to as the '*Neumann*' solution for the planar case. Instead of Eq. (6), we use Eq. (8) as an approximation for the case that $\left|\frac{c_i^{\mathrm{sol}}-c_i^0}{c_i^{\mathrm{part}}-c_i^{\mathrm{sol}}}\right| \ll 1$. This gives the following set of equations to be solved in k, c_1^{sol}, c_2^{sol}, …, c_n^{sol}.

$$\begin{cases} k = 2\,\dfrac{c_i^0 - c_i^{\mathrm{sol}}}{c_i^{\mathrm{part}} - c_i^{\mathrm{sol}}}\sqrt{\dfrac{D_i}{\pi}} \quad \text{for} \quad i\in\{1,\ldots,n\}, \\ (c_1^{\mathrm{sol}})^{m_1}(c_2^{\mathrm{sol}})^{m_2}(c_3^{\mathrm{sol}})^{m_3}(\ldots) = K \end{cases}. \tag{10}$$

Note that above equation is accurate whenever $\left|\frac{c_i^{\mathrm{sol}}-c_i^0}{c_i^{\mathrm{part}}-c_i^{\mathrm{sol}}}\right| \ll 1$. For cases where this inequality does not hold, then the above set of equations should be replaced by system (Eq. (9)). To illustrate the fact that more solutions can occur, we consider a *hypothetical* ternary alloy with $m_1 = 1 = m_2$, $c_1^{\mathrm{part}} = 50$, $c_2^{\mathrm{part}} = 1$, $c_1^0 = 2$ and $c_2^0 = 30$ and $D_2 = 2D_1$, then after some calculation one obtains two solutions for the interfacial concentrations and rate factor k

$$\begin{cases} c_1^{\mathrm{sol}} = 11.72680603, & c_2^{\mathrm{sol}} = 25.58241343, & k = -0.2867679473 \text{ 'slow' solution} \\ c_1^{\mathrm{sol}} = 42.43150941, & c_2^{\mathrm{sol}} = 7.070217490, & k = -6.027895861 \text{ 'fast' solution} \end{cases}.$$

Both solutions conserve mass and hence are well-posed. Note that the 'fast' solution does not satisfy $\left|c_i^{\mathrm{sol}} - c_i^0/c_i^{\mathrm{part}} - c_i^{\mathrm{sol}}\right| \ll 1$ and hence the use of above equations gives an inaccurate value for the 'fast' solution. We remark here that this has only been given for illustrational purposes. Real-world alloys do not fall into this class since the model is only valid in the dilute solution regime, i.e. $c_i \ll c_i^{\mathrm{part}}$, $i\in\{1,\ldots,n\}$ for $t>0$, $r\in\Omega(t)$. For the interested reader, we refer to [27] where several computations have been done to determine the two solutions for a ternary alloy. The same computations for the 'exact' *Neumann* solution are done in [27] in which the set of equations (Eq. (9)) is used instead of system (Eq. (10)). Furthermore, in [18] it has been shown that the interfacial velocity has the following upper and lower bound.

$$\frac{c_i^0 - c_i^{\mathrm{sol}}}{c_i^{\mathrm{part}} - c_i^{\mathrm{sol}}}\sqrt{\frac{D_i}{\pi t}} < \frac{\mathrm{d}S}{\mathrm{d}t} < \frac{c_i^0 - c_i^{\mathrm{sol}}}{c_i^{\mathrm{part}} - c_i^0}\sqrt{\frac{D_i}{\pi t}}. \tag{11}$$

This gives two easy bounds for the solution of the interfacial concentrations and hence the dissolution rate can be estimated very quickly.

3.2.2.1. The 'dilute' case. We consider the case that the particle concentration is much larger than the interface concentration. Furthermore, we assume that the initial concentration is almost equal to zero, i.e. $c_i^{\mathrm{part}} \gg c_i^{\mathrm{sol}} \gg c_i^0 \approx 0$. From the upper and lower bounds in above expression, it follows that the interface velocity can be approximated by

$$\frac{\mathrm{d}S}{\mathrm{d}t} = -\frac{c_i^{\mathrm{sol}}}{c_i^{\mathrm{part}}}\sqrt{\frac{D_i}{\pi t}} \quad \text{for} \quad i\in\{1,\ldots,n\}. \tag{12}$$

Since this has to hold for all $i\in\{1,\ldots,n\}$ it follows that all interfacial concentrations can be expressed in terms of, for instance, the interfacial concentration corresponding to the first element, i.e.

$$-\frac{c_i^{\mathrm{sol}}}{c_i^{\mathrm{part}}}\sqrt{D_i} = -\frac{c_1^{\mathrm{sol}}}{c_1^{\mathrm{part}}}\sqrt{D_1} \Rightarrow c_i^{\mathrm{sol}} = \frac{c_i^{\mathrm{part}}}{c_1^{\mathrm{part}}}\sqrt{\frac{D_1}{D_i}}\,c_1^{\mathrm{sol}}$$

We substitute all these expressions for c_i^{sol} into the hyperbolic relation for the interfacial concentrations (Eq. (1)) to obtain a simple exponential equation for c_1^{sol} whose non-negative real-valued solution gives

$$(c_1^{\mathrm{sol}})^{\mu}\left(\frac{c_2^{\mathrm{part}}}{c_1^{\mathrm{part}}}\sqrt{\frac{D_1}{D_2}}\right)^{m_2}\left(\frac{c_3^{\mathrm{part}}}{c_1^{\mathrm{part}}}\sqrt{\frac{D_1}{D_3}}\right)^{m_3}\cdots\left(\frac{c_n^{\mathrm{part}}}{c_1^{\mathrm{part}}}\sqrt{\frac{D_1}{D_n}}\right)^{m_n} = K$$

$$\Leftrightarrow c_1^{\mathrm{sol}} = \frac{c_1^{\mathrm{part}}}{\sqrt{D_1}}\left[\prod_{i=1}^{n}\left(\frac{\sqrt{D_i}}{c_i^{\mathrm{part}}}\right)^{m_i}K\right]^{1/\mu} (\in\mathbb{R}_0^+).$$

where $\Pi_{i=1}^n f_i := f_1 f_2$, …, f_n and $\mu := m_1 + m_2 + \cdots + m_n$. Note again that we consider only non-negative and real-valued concentrations. The solution for c_1^{sol} is substituted into Eq. (12) to obtain the interface velocity

$$\frac{\mathrm{d}S}{\mathrm{d}t} = -\frac{c_{\mathrm{eff}}^{\mathrm{sol}}}{c_{\mathrm{eff}}^{\mathrm{part}}}\sqrt{\frac{D_{\mathrm{eff}}}{\pi t}} \quad \text{with} \quad c_{\mathrm{eff}}^{\mathrm{sol}} := K^{1/\mu},$$
$$c_{\mathrm{eff}}^{\mathrm{part}} := \left[\prod_{i=1}^{n}(c_i^{\mathrm{part}})^{m_i}\right]^{1/\mu}, \quad D_{\mathrm{eff}} := \left[\prod_{i=1}^{n}(D_i)^{m_i}\right]^{1/\mu}. \tag{13}$$

We see that for this case particle dissolution in a multi-component alloy is mathematically reduced to particle dissolution in a binary alloy. The effective parameters (particle concentration and diffusion coefficient) are equal to geometric averages with weights according to stoichiometry. Above differential equation is solved to give the following dissolution time τ

$$\tau = \frac{\pi(c_{\mathrm{eff}}^{\mathrm{part}})^2 S_0^2}{4(c_{\mathrm{eff}}^{\mathrm{sol}})^2 D_{\mathrm{eff}}}.$$

We consider an example with three components. Let the particle concentrations of species 1 and 2 be equal, $c_1^{\mathrm{part}} = 33$ wt.% $= c_2^{\mathrm{part}}$, for the first two species. The particle concentration of the third component, c_3^{part}, is allowed to vary. When the stoichiometry is unchanged for all configurations, then the variation of the particle concentration reflects the molecular weight of the third component. Further, let the initial concentration in the

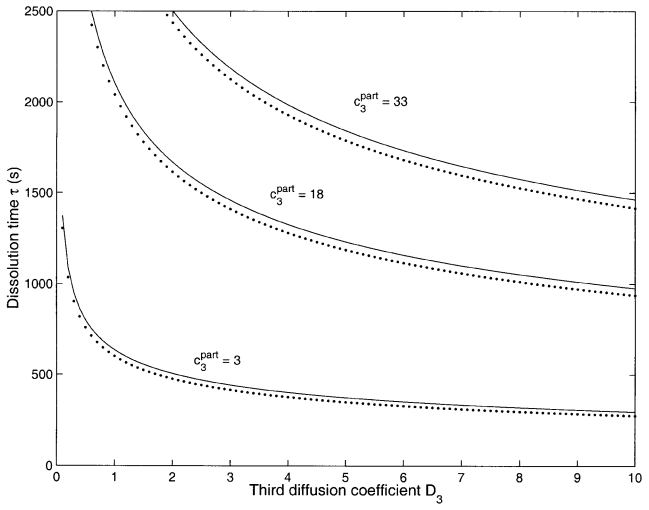

Fig. 3. The dissolution time τ as a function of the diffusion coefficient of the third element D_3 for consecutive values of the particle concentration of the third element c_3^{part}. The diffusion coefficient and time are given in the units $\mu m^2\ s^{-1}$ and s. The solid and dotted curves, respectively, correspond to the approximate solution and the exact solution.

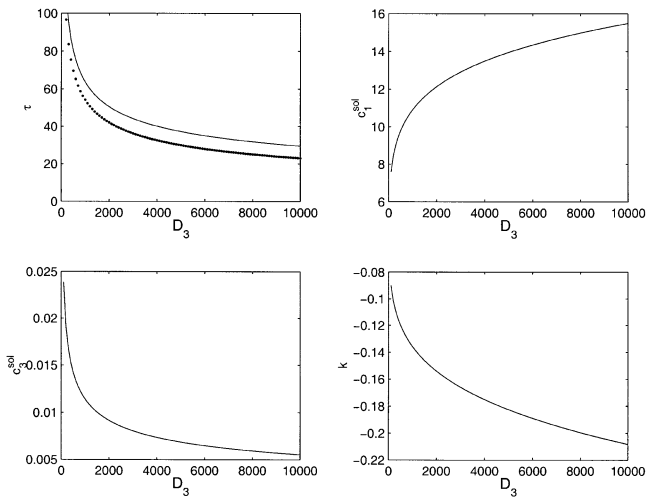

Fig. 4. Top-left, the dissolution time as a function of the diffusion coefficients of the third component for larger values. The dotted and solid lines, respectively, correspond to the exact and approximate solution. Top-right, the interfacial concentration of the first component as a function of the diffusion coefficient of the third component. Bottom-left, the interfacial concentration as a function of the diffusion coefficient of the third component. Bottom-right, the velocity coefficient k as a function of the diffusion coefficient of the third component. Calculations have done with particle concentrations of 33 for the first two components, the particle concentration of the third component is 3.

matrix be zero for all alloying elements, i.e. $c_i^0 = 0$. The solubility product is chosen equal to one, i.e. $K = 1$. We start with a layer of thickness $S_0 = 10^{-6}$ m. This data-set gives $c_{\text{eff}}^{\text{sol}} = 1$. We start with diffusivities $D_1 = 10^{-13}$ m^2 s^{-1} and $D_2 = 2 \times 10^{-13}$ m^2 s^{-1}. The third diffusion coefficient is allowed to vary to study its impact on the dissolution time. As can be seen from substitution into above relation, the dissolution time $\tau(s)$ varies with the diffusion coefficient of the third component according to a reciprocal power of one third, i.e. $\tau \propto (D_3)^{-1/3}$. Fig. 3 shows the variation of the dissolution time with the value of the third diffusion coefficient for relatively low values. Both the approximate solution, based on Eq. (12), and the 'exact' *Neumann* solution of system (Eq. (9)), are plotted in Fig. 3 for consecutive particle concentrations. It can be seen that the difference is small.

From Fig. 3, it can be seen that the dissolution time is highly sensitive to changes of the diffusion coefficient of the third component, D_3, when D_3 is small. A small value of D_3 corresponds to the addition of a slowly diffusing third component. Hence dissolution times are long when a slowly diffusing third component is added. Furthermore, it can be seen from Fig. 3 that the dissolution time increases for increasing particle concentration of the third component.

Fig. 4 shows a similar picture in the top-left as in Fig. 3, however, the diffusion coefficient of the third component is varied over a larger range and the particle concentration of the third component is set equal to 3, i.e. $c_3^{\text{part}} = 3$ wt.%. In Fig. 4, we see that the interfacial concentration of the first component increases for increasing D_3. Hence, the difference $c_1^{\text{part}} - c_1^{\text{sol}}$ decreases and therewith $\left|c_1^{\text{sol}} - c_1^0 / c_1^{\text{sol}} - c_1^0\right|$ increases and hence $\left|c_1^{\text{sol}} - c_1^0 / c_1^{\text{sol}} - c_1^0\right| \ll 1$ is no longer true. However, the interfacial concentration of the second component decreases and hence $\left|c_1^{\text{sol}} - c_1^0 / c_1^{\text{sol}} - c_1^0\right| \ll 1$ decreases. This implies that these two effects work against each other, and this supports the small difference between the exact '*Neumann*' solution and approximate solution (Eq. (11)), also for high values of D_3. Note, however, that the difference in Fig. 4 is more significant than in Fig. 3. For completeness, we also give the evolution of the velocity coefficient, k, as a function of the diffusion coefficient of the third component.

When we increase the diffusion coefficient D_3 sufficiently, then c_1^{sol}, as predicted by Eq. (11) exceeds the value of c_1^{part}. Therewith, one enters the region of ill-posedness (mass is no longer conserved). Of course Eq. (11) cannot be used for this case. So this behaviour of $\tau \propto (D_3)^{-1/3}$ breaks down for large D_3. This breakdown takes place when c_1^{sol} becomes significant with respect to c_1^{part}. Eq. (10) is used as an initial guess for the 'exact' *Neumann* solution (Eq. (9)), obtained from numerical solution of this system. We also observed that when c_1^{sol}, as determined from approximation (Eq. (11)) and used as an initial guess for the solution of Eq. (6), exceeds c_1^{part} no convergence is obtained when Eq. (6) is solved numerically. It is shown in [27] that also no *Neumann* solutions exist in this range.

In Figs. 3 and 4, we see that the dissolution time as predicted by the *Neumann* solution is smaller than for the quasi-binary approach. This is explained as follows: consider Eq. (6), we see that convergence to Eq. (7)

takes place as $D_3 \to \infty$. Since $c_i^0 = 0$ and $c_i^{\mathrm{sol}} \geq 0$ it follows that $(c_1^{\mathrm{sol}} - c_1^0 / c_1^{\mathrm{part}} - c_1^{\mathrm{sol}}) = (\frac{c_i^{\mathrm{sol}}}{c_i^{\mathrm{part}} - c_i^{sol}}) < (\frac{c_i^{\mathrm{sol}}}{c_i^{\mathrm{part}}})$. Use of Eq. (8) shows that the *Neumann* solution time is smaller than the quasi-binary dissolution time for D_3 sufficiently large. Hence, $\tau \to 0$ as $D_3 \to \infty$.

We define the relative error made by the use of the quasi-binary approach as

$$\epsilon := \frac{|\tau_{\mathrm{N}} - \tau_{\mathrm{qb}}|}{\tau_{\mathrm{N}}},$$

where τ_{N} and τ_{qb}, respectively, correspond to the dissolution time as predicted by the use of the *Neumann* solution and the quasi-binary approach. We plot the relative error made by the use of the quasi-binary approach as a function of the diffusion coefficient for different particle concentrations in Fig. 5 on a double logarithmic scale. It can be seen that the relative error increases monotonically with D_3. Furthermore, the relative error increases as the particle concentration of the third component decreases. This is explained by the increase of the significance of the interfacial concentration. The slope of all lines for consecutive particle concentrations is the same. This suggests an approximate power behaviour for the relative error $\epsilon \propto (D_3)^{0.42}$.

When the assumption $0 \approx c_i^0 \ll c_i^{\mathrm{sol}} \ll c_i^{\mathrm{part}}$ is relaxed, both expressions in Eq. (10) can be combined to get a polynomial equation of order $\mu = m_1 + m_2 + \ldots + m_n$ in c_1^{sol}. A numerical zero-point method can be used to get the solution. This more general case is omitted here, since we are not able to find *general* expressions for the zeros of the resulting polynomial.

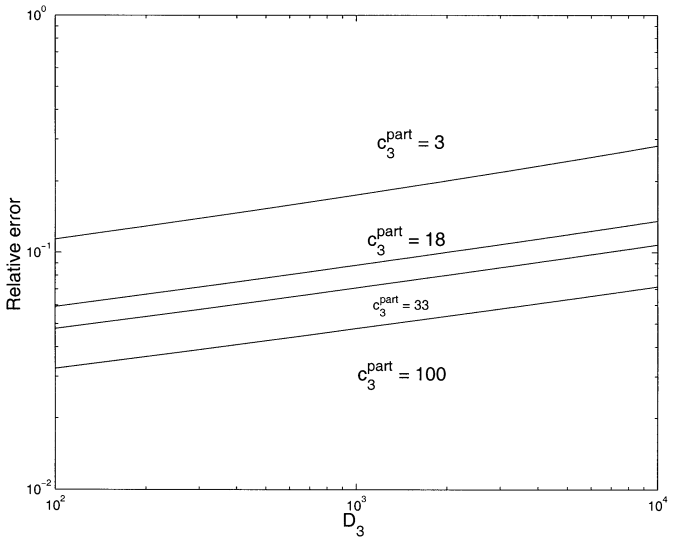

Fig. 5. The relative error of the dissolution time as predicted by the quasi-binary approach as a function of the diffusion coefficient of the third component for consecutive particle concentrations.

3.3. An asymptotic solution for the spherical case

The diffusion equation for the spherical case in an unbounded domain admits a similar self-similar solution, in terms of $c = c(r/\sqrt{t})$, as for the planar case. However, one obtains incompatibility with the interface rate equation. Therefore, we are not able to find a solution of the type of the previous section. Using Laplace transforms, Whelan [4] came up with the following expression for the interface velocity

$$\frac{\mathrm{d}S}{\mathrm{d}t} = -\frac{c_i^{\mathrm{sol}} - c_i^0}{c_i^{\mathrm{part}} - c_i^{\mathrm{sol}}}\left\{\frac{D_i}{S} + \sqrt{\frac{D_i}{\pi t}}\right\}. \tag{14}$$

The interfacial position $S(t)$ has been treated as a constant during Whelan's derivation. At early stages it behaves like Aaron and Kotler's [10] solution, i.e. the second (planar) term dominates. At later stages as the second term decreases, the first term becomes more important during dissolution. Therefore, at some stage, say $t_1 < t < t_2$, we approximate the interfacial velocity by

$$\frac{\mathrm{d}S}{\mathrm{d}t} = -\frac{c_i^{\mathrm{sol}} - c_i^0}{c_i^{\mathrm{part}} - c_i^{\mathrm{sol}}}\frac{D_i}{S}. \tag{15}$$

Above equation is also obtained after solving of the stationary diffusion and subsequent substitution of this solution into the Stefan condition. We remark that this solution becomes inaccurate again as blow up ($|\mathrm{d}S/\mathrm{d}t| \to \infty$ as $S \to 0$) takes place. Similar to the planar case we assume $0 \approx c_i^0 \ll c_i^{\mathrm{sol}} \ll c_i^{\mathrm{part}}$. After carrying out the same analysis as before for the planar case, we see all interfacial concentrations can be expressed in terms of the interfacial concentration of the first element

$$c_i^{\mathrm{sol}} = -\frac{c_i^{\mathrm{part}} D_1}{c_1^{\mathrm{part}} D_i} c_1^{\mathrm{sol}} \quad \text{for } i \in \{1, \ldots, n\}.$$

Substitution of above relations into the hyperbolic relation for the interfacial concentrations (Eq. (1)) gives the following expression for the interfacial concentration of the first alloying element

$$c_1^{\mathrm{sol}} = -\frac{c_1^{\mathrm{part}}}{D_1}\left[\prod_{i=1}^{n}\left(\frac{D_i}{c_i^{\mathrm{part}}}\right)^{m_i} K\right]^{1/\mu} \quad \text{with}$$

$$\mu := m_1 + m_2 + \ldots + m_n.$$

Above expression is similar to the one for planar geometry except for the absence of the square root for the diffusion coefficients. This gives hence different values for the interfacial concentrations c_i^{sol}. So during the dissolution process the values of the interfacial concentrations converge from the values as determined in the previous section to the values just mentioned. Note that this holds for the case that the interfacial position moves slowly, i.e. $|(c_i^{\mathrm{sol}} - c_i^0)/(c_i^{\mathrm{part}} - c_i^{\mathrm{sol}})| \ll 1$. Let the time be in the interval $t_1 < t < t_2$, then substitution of above expression into Eq. (15) gives for the interfacial velocity

$$\frac{\mathrm{d}S}{\mathrm{d}t} = -\frac{c_1^{\mathrm{sol}}}{c_1^{\mathrm{part}}}\frac{D_1}{S} \Rightarrow \frac{\mathrm{d}S}{\mathrm{d}t} = -\frac{c_{\mathrm{eff}}^{\mathrm{sol}}}{c_{\mathrm{eff}}^{\mathrm{part}}}\frac{D_{\mathrm{eff}}}{S}.$$

where the effective interfacial concentration, particle concentration and diffusion coefficient are defined by $c_{\mathrm{eff}}^{\mathrm{sol}} := K^{1/\mu}$, $c_{\mathrm{eff}}^{\mathrm{part}} := [\Sigma_{i=1}^{n}(c_i^{\mathrm{part}})^{m_i}]^{1/\mu}$, $D_{\mathrm{eff}} := [\Sigma_{i=1}^{n}(D_i)^{m_i}]^{1/\mu}$. Solution of above equation is trivial. Note that these effective parameters are equal to the ones that were obtained for the planar case. Nevertheless, the interfacial concentrations differ in both cases. Furthermore, it should be noted that the approximations hold under limiting assumptions.

For the more general case, where $0 \approx c_i^0 \ll c_i^{\mathrm{sol}} \ll c_i^{\mathrm{part}}$ does not hold necessarily and where we are in the range of time where both terms in Eq. (14) are of same order, the interfacial concentrations are continuous functions of time. Their values start at the planar solution (see preceding subsection) and converges towards the solution obtained in this subsection (see above relation). The evolution of the interfacial concentrations and interfacial position is obtained by the use of the full Eq. (14) and hyperbolic relation (Eq. (1)) for the interfacial concentrations. The calculation of the interfacial concentrations is straightforward.

4. Numerical method

Various numerical methods are known to solve Stefan-problems, front-tracking; front-fixing and fixed domain methods. Since the concentration at the interface varies with time in our problem, we restrict ourselves to a front-tracking method. Recently a number of promising methods are proposed for multi-dimensional problems, phase field methods and level set methods, such as in Eqs. (1) and (2). However, imposing local equilibrium condition at the interface in such models is not as straightforward as in front-tracking methods that are used here. A coupling between thermodynamics and a phase field model is presented by Grafe et al. [28].

Our main interest is to give an accurate discretisation of the boundary conditions for this Stefan-problem with one spatial co-ordinate. Therefore, we use the classical moving grid method of Murray and Landis [29] to discretise the diffusion equations. In this paper we briefly describe the method, for more details we refer to [18].

4.1. Discretisation of the interior region

We use an implicit finite difference method to solve the diffusion equation in the inner region. An explicitly treated convection term due to grid-movement is included. Since the magnitude of the gradient is maximal near the moving interface we use a geometrically distributed grid such that the discretisation near the interface is fine and coarse farther away from the moving interface. Furthermore, we use a virtual grid-point near the moving boundary. The distance between the virtual node and the interface is chosen equal to the distance between the interface and the first grid-node. The resulting set of linear equations is solved using a tridiagonal matrix solver.

4.2. Discrete boundary conditions at the interface

We define the discrete approximation of the concentration as $c_{i,k}^{j}$, where j, i and k, respectively, denote the time-step, the index of the chemical (alloying) element and gridnode. The virtual gridnode behind the moving interface and the gridnode at the interface, respectively, have indices $k = -1$ and $k = 0$. At the moving interface, we obtain from discretisation of Eq. (4)

$$\frac{D_i}{c_i^{\mathrm{part}} - c_i^{\mathrm{sol}}}\frac{c_{i,1}^{j+1} - c_{i,-1}^{j+1}}{2\Delta r} = \frac{D_{i+1}}{c_{i+1}^{\mathrm{part}} - c_{i+1}^{\mathrm{sol}}}\frac{c_{i+1,1}^{j+1} - c_{i+1,-1}^{j+1}}{2\Delta r},$$

$$\text{for } j \in \{1, \ldots, n-1\}.$$

Note that the concentration profile of each element is determined by the value of the interfacial concentration. Above equation can be re-arranged into a zero-point equation for all chemical elements. All interfacial concentrations satisfy the hyperbolic relation (Eq. (1)). Combination of all this, gives for $i \in \{1, \ldots, n-1\}$ and $i = n$

$$f_i(c_{i,0}^{j+1}, c_{i+1,0}^{j}) := D_i(c_{i,1}^{j+1} - c_{i,-1}^{j+1})(c_{i+1}^{\mathrm{part}} - c_{i+1}^{\mathrm{sol}}) - D_{i+1}(c_{i+1,1}^{j+1} - c_{i+1,-1}^{j+1})(c_i^{\mathrm{part}} - c_i^{\mathrm{sol}}) = 0.$$

$$f_n(c_1^{\mathrm{sol}}, \ldots, c_n^{\mathrm{sol}}) := (c_1^{\mathrm{sol}})^{m_1}(c_2^{\mathrm{sol}})^{m_2}(\ldots)(c_n^{\mathrm{sol}})^{m_n} - K = 0.$$

To approximate a root for the 'vector-function' f we use Newton's method combined with discrete approximations for the non-zero entries in the first $n-1$ rows of the Jacobian matrix. The iteration is terminated when sufficient accuracy is reached. This is explained in more detail in [18].

4.3. Adaptation of the moving boundary

The moving interface is adapted according to Eq. (4). In [30] the forward (explicit) Euler and Trapezium time integration methods are described and compared. It was found that the (implicit) Trapezium method was superior in accuracy. Furthermore, the iteration step to determine the interfacial concentrations is included in each Trapezium step to determine the interfacial position. Hence, the work per time-iteration remains the same for both time-integration methods. Therefore, the Trapezium rule is used to determine the interfacial position as a function of time. We terminate the iteration when sufficient accuracy is reached, i.e. let ε be the inaccuracy, then we stop the iteration when the inequality

$$\sum_{i=1}^{n} |c_i^{\mathrm{sol}}(p+1) - c_i^{\mathrm{sol}}(p)| + \frac{|S^{j+1}(p+1) - S^{j+1}(p)|}{S^{j+1} - M} < \varepsilon$$

Table 1
Input data

Physical quantity	Value	SI-unit
D_1	10^{-13}	$m^2\ s^{-1}$
D_2	2×10^{-13}	$m^2\ s^{-1}$
K	1	–
c_1^{part}	33	–
c_2^{part}	33	–
c_1^0	0	–
c_2^0	0	–
c_3^0	0	–
m_1	1	–
m_2	2	–
S_0	10^{-6}	M
M	10^{-4}	M

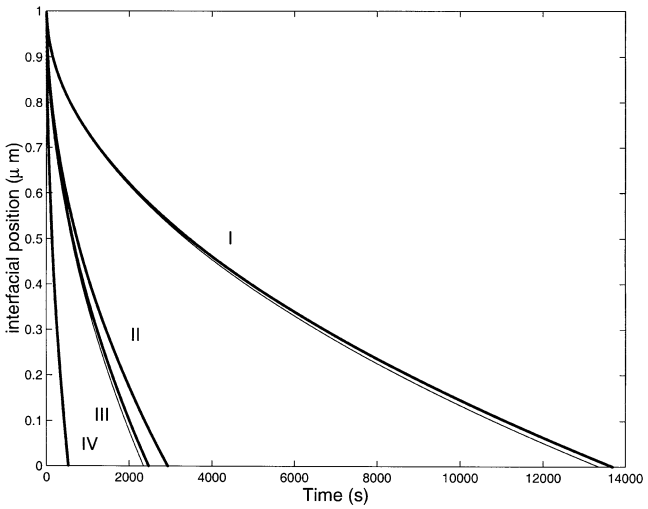

Fig. 6. The interfacial position as a function of time. All curves correspond to the configuration as listed in Table 1. The bold and ordinary curves, respectively, reflect the quasi-binary and full multi-component solution. Curves I corresponds to $c_3^{part}=33$ and $D_3=0.1\times10^{-13}$. Curve II reflects the case that $c_3^{part}=3$ and $D_3=0.1\times10^{-13}$. Curve III displays the situation in which $c_3^{part}=33$ and $D_3=10\times10^{-13}$, whereas curve IV shows the configuration $c_3^{part}=3$ and $D_3=10\times10^{-13}$.

holds. Here, S^j denotes the discrete approximation of the interfacial position at time-step j. The integer p represents the iteration number during the determination of the interfacial concentrations and position.

5. Numerical experiments

This section contains the numerical experiments done with the finite difference method. We aim at a comparison between the quasi-binary solution and the full multi-component solution. Experiments are done for planar and spherical geometries. The input-data used is hypothetical but the order of magnitude is comparable to the case of commercial aluminium alloys.

5.1. Planar experiments

We consider the quasi-binary and multi-component approach for the planar geometry. The configuration entered here applies to a quaternary alloy. As input-data we use the values as listed in Table 1.

We vary the diffusion coefficient and particle concentration of the third component (D_3 and c_3^{part}). The results are shown in Fig. 6 where we plot the interfacial position as a function of time. For all these situations, it can be seen that the quasi-binary solution and full multi-component solution agree very well (see Fig. 6). This agreement persists also for the higher diffusivities of the third alloying element. This is in agreement with the result shown in Fig. 4 for the case that the region is unbounded.

Furthermore, one expects that the concentration at the cell boundary (i.e. at $r=M$) is larger for cases where the diffusion coefficient of the third component is larger. However, both the penetration depth and the interfacial position exhibit a square-root behaviour with time. This implies that possibly the atoms from the alloying elements reach the cell boundary M after complete dissolution of the particle. This depends on the cell size and geometry. Therefore, the observed differences in dissolution rate remain small for all cases where the geometrical settings are equal.

Fig. 7 shows the same configuration as in Table 1 with $c_3^{part}=33$ and $D_3=10\times10^{-13}$ except all curves correspond to cell sizes $M=5\times10^{-5}$ and $M=2.5\times10^{-5}$. The bold lines correspond to the full multi-component solution. Whereas the other lines are predicted using the quasi-binary approach. It can be seen that the difference between the quasi-binary approach and full multi-component approach is more significant. This significant difference has also been observed when non-zero values for the initial concentrations are taken.

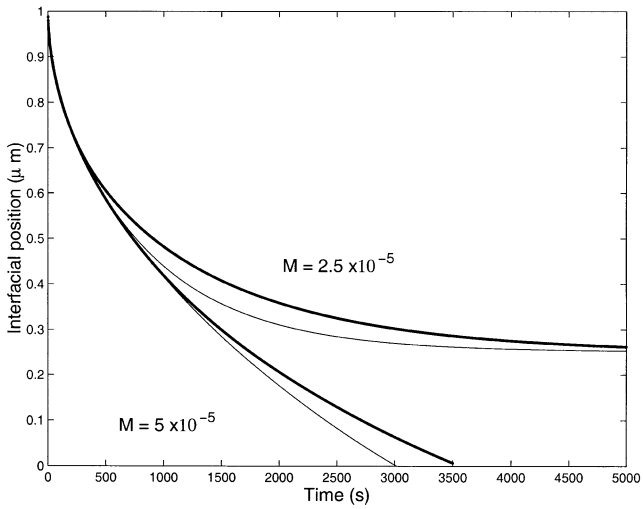

Fig. 7. The interfacial position as a function of time. The bold curve corresponds to the multi-component approach.

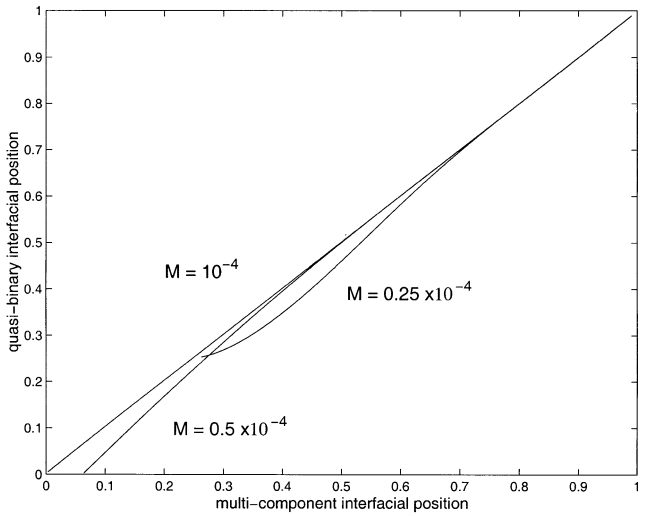

Fig. 8. The computed interfacial position by the quasi-binary approach as a function of the computed interfacial position using the full multi-component approach for consecutive cell-sizes.

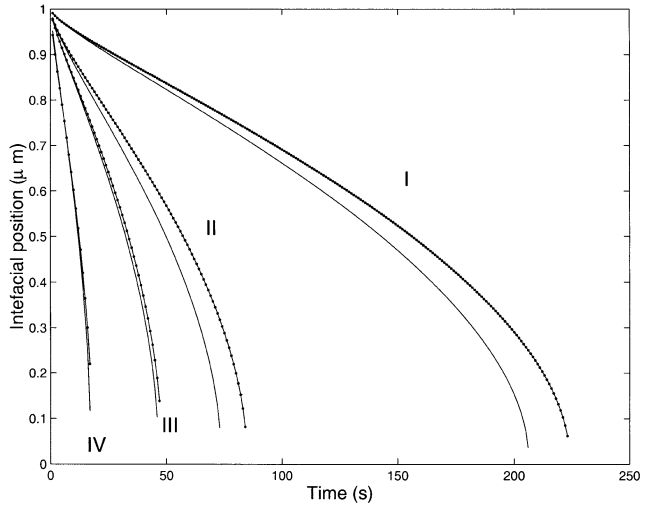

Fig. 9. The interfacial position as a function of time for a spherical dissolving particle. All curves correspond to the input-data from Table 1. The bold and ordinary curve, respectively, correspond to the quasi-binary and full multi-component approaches. Curves I correspond to $c_3^{\text{part}} = 33$ and $D_3 = 10^{-14}$. Curves II depict the case that $c_3^{\text{part}} = 3$ and $D_3 = 10^{-14}$. The situation with $c_3^{\text{part}} = 33$ and $D_3 = 10^{-12}$ is shown by curve III. Whereas curves IV display the case that $c_3^{\text{part}} = 3$ and $D_3 = 10^{-12}$.

Fig. 8 presents the interfacial position as computed by the quasi-binary approach as a function of the computed interfacial position by the full multi-component approach. It can be seen that the curvature of the line increases for smaller cell-sizes. This is attributed to the accumulation of the atoms of the alloying elements at the cell boundary. For the case of $M = 2.5 \times 10^{-5}$ an interesting behaviour is observed. At the early stages where the atoms did not reach the cell-boundary yet, the curve is straight. Later, as the atoms reach the cell-boundary, the curve starts to deviate from a straight line, similar to the case of a cell-boundary at $M = 5 \times 10^{-5}$. Subsequently, the matrix gets saturated and dissolution stops, the dissolution rate converges towards zero. The equilibrium state is not effected by the use of the quasi-binary approach and the thereby the curve converges back to the straight line.

5.2. Spherical experiments

We consider the dissolution of a spherical particle in the multi-component and quasi-binary alloy. The configuration entered here applies to a quaternary alloy. We use the same input-data from Table 1, except for the geometry and the cell size, $M = 10^{-5}$, unless stated otherwise. We vary the particle concentration and diffusion coefficient of the third component.

For different diffusivities and particle concentrations of the third component, the results are shown in Fig. 9. The agreement between the quasi-binary approach and the full multi-component solution is good. The difference between the two approaches is smallest for the higher values of the diffusion coefficient of the third component. As expected, the dissolution process takes place relatively fast compared with the rate of penetration of the alloying elements from the particle into the matrix, although the order of magnitude of the rate of both processes is similar. Let S_{mc} and S_{qb} be the interfacial positions predicted using, respectively, the multi-component and quasi-binary approach. We compare the relative errors, defined by

$$\epsilon := \frac{|S_{\text{mc}} - S_{\text{qb}}|}{S_{\text{mc}}} \times 100\%$$

taken at the times when the multi-component solution is nearest to $S_{\text{mc}} = 0.5$, we see that the errors for the cases corresponding to curves I–IV in Fig. 9 are, respectively, given by 9.94, 13.90, 4.23 and 3.87%. It can be seen that the quasi-binary approach is most accurate for cases where the diffusion coefficient of the third component is large. This observation is contrary to Fig. 5 where the error becomes more significant for larger diffusion coefficients of the third component. This discrepancy may be caused by the geometrical differences between this situation and the situation in Fig. 5 (sphere and bounded domain vs. plane and unbounded).

Some dissolution curves are shown in Fig. 10 for different values of the cell radius. Here we took a low value for the diffusion coefficient of the third component, being a case where the quasi-binary approach is less accurate (compared with the case where the diffusion coefficient of the third component is high). It can be seen that the difference between the quasi-binary and full multi-component approach is reasonably small. However, for the case that $M = 4 \times 10^{-6}$ the difference

is large. Apparently, the difference between both approaches is large when dissolution times are large, but finite. In the case that $M = 2.5 \times 10^{-6}$ full dissolution does not take place. The difference between the different approaches is large at early stages, but becomes less significant as time proceeds; the curves reach the same limit. This observation is similar to the observation in the planar case (see Fig. 8). We remark that this observation follows from experiment and that a more mathematical basis is needed for a full understanding.

Finally, we show the interfacial position as a function of time for different initial matrix concentrations in Fig. 11. For low initial matrix concentrations, the difference between the quasi-binary and full multi-component approach is small. For larger concentrations, the difference increases and hence the quasi-binary approach breaks down. This is attributed to the fact that the difference between the interfacial concentration and initial concentration becomes more significant (see Eq. (15)).

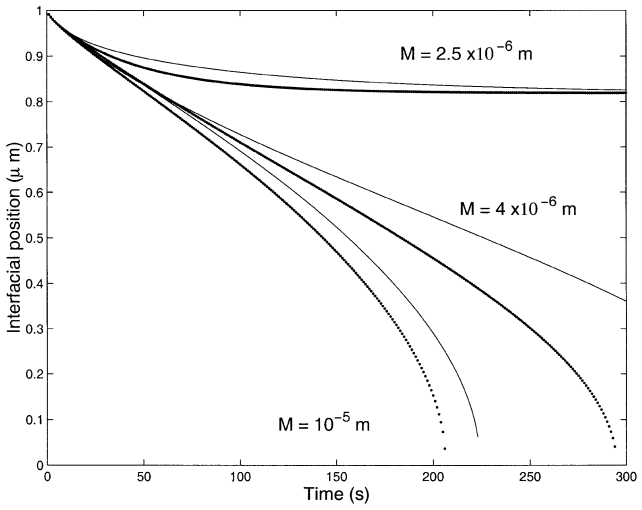

Fig. 10. The interfacial position as a function of time for a spherical dissolving particle for consecutive cell radii. The bold curves correspond to the quasi-binary approach. The configuration is taken from Table 1 $c_3^{\text{part}} = 33$ and $D_3 = 10^{-14}$.

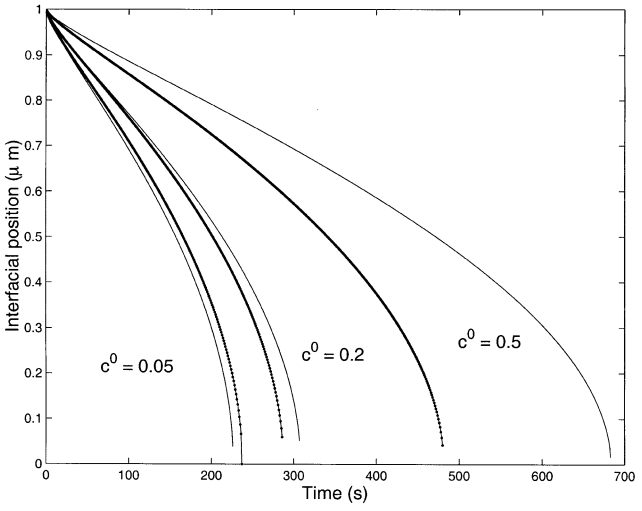

Fig. 11. The interfacial position as a function of time for a spherical dissolving particle for consecutive initial matrix concentrations. The bold curves correspond to the quasi-binary approach. The configuration is taken from Table 1 with $c_3^{\text{part}} = 33$ and $D_3 = 10^{-14}$.

6. Conclusions

A model, based on a vector-valued Stefan-problem, has been developed to predict the dissolution of particles in general multi-component alloys. A remark has been given concerning existence and well-posedness of solutions of the vector-valued Stefan-problem. The remark is motivated using a physical argument. For general cases with one spatial co-ordinate the full vector-valued Stefan-problem is solved using finite differences.

For some cases, when the difference between the particle concentrations and interfacial concentrations are large and when the initial matrix concentration is negligible, the full multi-component (vector-valued) Stefan-problem can be approximated accurately using an averaging technique for the particle concentrations and diffusion coefficients. This reduces the multi-component problem to a quasi-binary problem. This approximation is essentially useful when more geometric flexibility is included into the model (see for instance [7,14]). It also turned out that this quasi-binary approach is accurate for the spherical dissolving phases. We expect this method also to be accurate for the case of dissolving cylindrical phases in multi-component alloys.

Acknowledgements

We thank one of the referees for his remarks, which improved the manuscript.

References

[1] W. van Til, C. Vuik, S. van der Zwaag, An inventory of numerical methods to model solid–solid phase transformations in aluminium alloys, NIMR-report, P.004.001, 2000.
[2] R. Kobayashi, Phys. D 63 (1993) 410–423.
[3] J. Ågren, J. Phys. Chem. Solids 43 (1981) 421–430.
[4] M.J. Whelan, Met. Sci. J. 3 (1969) 95–97.
[5] U.L. Baty, R.A. Tanzilli, R.W. Heckel, Met. Trans. 1 (1970) 1651–1656.
[6] U.H. Tundal, N. Ryum, Met. Trans. 23A (1992) 433–449.
[7] G. Segal, C. Vuik, F.J. Vermolen, J. Comp. Phys. 141 (1998) 1–21.
[8] F.J. Vermolen, P. van Mourik, S. van der Zwaag, Mater. Sci. Technol. 13 (1997) 308–313.

[9] F.N. Nolfi Jr, P.G. Shewmon, J.S. Foster, Trans. Met. Soc. AIME 245 (1969) 1427–1433.
[10] H.B. Aaron, G.R. Kotler, Met. Trans. 2 (1971) 1651–1656.
[11] F.J. Vermolen, S. van der Zwaag, Mater. Sci. Eng. A220 (1996) 140–146.
[12] G.P. Krielaart, Primary ferrite formation from supersaturated austenite, Thesis, Delft University of Technology, the Netherlands, 1995.
[13] Y. van Leeuwen, Moving interfaces in low-carbon steel, Thesis, Delft University of Technology, the Netherlands, 2000.
[14] C. Vuik, G. Segal, F.J. Vermolen, J. Comp. Vis. Sci. 3 (2000) 109–114.
[15] S.P. Chen, M.S. Vossenberg, F.J. Vermolen, J. van der Langkruis, S. van der Zwaag, Mater. Sci. Eng. A272 (1999) 250–256.
[16] O. Reiso, N. Ryum, J. Strid, Met. Trans. A 24A (1993) 2629–2641.
[17] R. Hubert, ATB Met. 34–35 (1995) 4–14.
[18] F.J. Vermolen, C. Vuik, J. Comp. Appl. Math. 126 (2001) 233–254.
[19] F.J. Vermolen, C. Vuik, S. van der Zwaag, Mater. Sci. Eng. A254 (1998) 13–32.
[20] F.J. Vermolen, C. Vuik, S. van der Zwaag, Mater. Sci. Eng. A246 (1998) 93–103.
[21] J.S. Kirkaldy, D.J. Young, Diffusion in the Condensed State, The Institute of Metals, London, 1987.
[22] J. Crank, Free and Moving Boundary Problems, Clarendon Press, Oxford, 1984.
[23] J. Chadam, H. Rasmussen, Free Boundary Problems Involving Solids, Longman, Harlow, London, 1993.
[24] A. Visintin, Models of Phase Transitions, Progress in Non-linear Differential Equation and Their Application, vol. 38, Birkhäuser, Boston, 1996.
[25] M.H. Protter, H.F. Weinberger, Maximum Principles in Differential Equations, Prentice-Hall, Englewood Cliffs, NJ, 1967.
[26] H. Weber, Die partiellen Differential-Gleichungen der Mathematischen Physik, Vieweg, Braunschweig, 1901.
[27] F.J. Vermolen, C. Vuik, Nieuw Archief voor Wiskunde 17 (1999) 205–217.
[28] U. Grafe, B. Böttger, J. Tiaden, S.G. Fries, Scr. Mater. 42 (2000) 1179–1186.
[29] W.D. Murray, F. Landis, Trans. ASME (C) J. Heat Transfer 245 (1959) 106–112.
[30] F.J. Vermolen, C. Vuik, J. Comp. Appl. Math. 93 (1998) 123–143.